Repeated low-intensity focused ultrasound led to microglial profile changes in TgF344-AD rats.

Laurene Abjean[1,2], Anthony Novell[3], Benoît Larrat[4], Boris Rafael Gueorguiev[2], Thomas Cailly[5,6,7,8], Christine Fossey[7], Frédéric Fabis[7], Rares Salomir[2,9], Stergios Tsartsalis[1,2], Benjamin B. Tournier[1,2], Philippe Millet[1,2*], Kelly Ceyzériat[10*]

[1]Department of Psychiatry, University Hospitals of Geneva, Geneva, Switzerland.

[2]Faculty of Medicine, University of Geneva, Geneva, Switzerland.

[3]Laboratoire d'Imagerie Biomédicale Multimodale (BioMaps), Université Paris-Saclay, CEA, CNRS, Inserm, Service Hospitalier Frédéric Joliot, 4 place du Général Leclerc, 91401 Orsay, France

[4]Neurospin, Institut Joliot, Direction de la Recherche Fondamentale, CEA, Université Paris Saclay, 91190 Gif sur Yvette, France

[5]Université de Caen Normandie, CERMN UR 4258, 14000 Caen, France.

[6]Department of Nuclear Medicine, CHU Cote de Nacre, 1400 Caen, France

[7]Université de Caen Normandie, CYCERON UAR 3408-US50, IMOGERE, 14000 Caen, France.

[8]Institut Blood and Brain @Caen-Normandie (BB@C) Boulevard Henri Becquerel, 14074 Caen, France.

[9]Radiology Department, University Hospitals of Geneva, Geneva, Switzerland

[10]CIBM Center for Biomedical Imaging, Geneva, Switzerland.

[*] These authors equally contributed to this work.

Corresponding author:
Kelly Ceyzériat, PhD
CIBM Center for Biomedical Imaging
University of Geneva
Avenue de la Roseraie, 64
1205 Geneva
Switzerland
Tel.: +41 22 379 46 56
Kelly.ceyzeriat@unige.ch

Abstract

Alzheimer's disease (AD), the most common cause of dementia, represents one of the main clinical challenges of the century as the number of patients is predicted to triple by 2050. Despite the recent approval of three monoclonal antibodies targeting Amyloid β (Aβ) aggregates by the Food and Drug Administration (FDA), immunotherapies still face challenges due to the difficulty of antibodies crossing the blood-brain barrier (BBB). This necessitates administering large doses of drugs to achieve their therapeutic effects, which is associated with significant side effects. In this context, low-intensity focused ultrasound (LiFUS) appears as an innovative and non-invasive method which, in association with intravenous injection of microbubbles (MB), leads to a transient BBB opening. This innovative strategy has been extensively studied in different preclinical models and more recently in human clinical trials, particularly in the context of AD. LiFUS+MB seems to increase the inflammatory response at short term, but the time course of this response is not consistent between studies, certainly due to the discrepancy between LiFUS protocols used. Moreover, the impact at longer term is understudied and the mechanisms underlying this effect are still not well understood. In our study, we therefore used the TgF344-AD rat model of AD, to investigate the effect of a single or multiple exposures to LiFUS+MB in the entire brain, on inflammatory response and amyloid load. The ultrasound attenuation through the skull was corrected to apply a peak negative acoustic pressure of 450 kHz in all treated animals. Single LiFUS+MB exposure induces a slight astrocyte and microglial response 24 hours post-treatment whereas repeated LiFUS treatment seems to induce microglial reprogramming, leading to the adaptation of gene expression related to key functions such as inflammatory response, mitochondrial and energetic metabolism. In our rat model and LiFUS+MB protocol conditions, multiple exposures did not modulate soluble/poorly aggregated forms nor the highly aggregated forms of $A\beta_{40}$ and $A\beta_{42}$. For therapeutic AD management, LiFUS+MB could be combined with drugs such as immunotherapies. In a proof-of-concept experiment, we validated that LiFUS was also efficient to improve the brain entry of the anti-Aβ antibody, Aducanumab.

Keywords: Low-intensity ultrasound, microglia, neuroinflammation, amyloid, Alzheimer's

Introduction

Alzheimer's disease (AD), one of the main causes of dementia, is associated at the neuropathological level with amyloid plaques and tauopathy. The amyloid pathology is due to extracellular aggregation of soluble amyloid beta (Aβ) monomers into oligomers, fibrils, protofibrils and finally amyloid plaques. The tauopathy is mainly observed in neurons due to hyperphosphorylated tau protein aggregation. Classical hallmarks of the disease also include a neuroinflammatory response involving astrocytes and microglial cells. When they become reactive, both cell types demonstrate morphological, transcriptional and functional modifications directly impacting the pathology[1,2].

Despite intensive research for treatments, most existing drugs only slow disease progression and alleviate symptoms. Recently, three monoclonal antibodies, Aducanumab (Adu, Biogen and Eisai), Lecanemab (Biogen and Eisai), and Donanemab (Lilly), targeting different forms of Aβ aggregates[3,4] have been approved by the Food and Drug Administration (FDA) as new treatments for AD, the first in nearly two decades[5]. Clinical trials have demonstrated that these treatments can reduce Aβ levels and improve cognition in patients with prodromal or mild AD, with effects varying based on dosage and duration of treatment[5-7]. Unfortunately, those immunotherapies require a large dose infusion of antibody due to blood-brain barrier (BBB) blockage which could be associated with important side effects such as amyloid-related imaging abnormalities (ARIA), whose occurrence may dependent on the dosage[8,9] and does not seem to be limited to anti-amyloid therapies[10]. Consequently, many studies are investigating strategies to enhance the entry of therapeutic molecules into the brain, to reduce the injected peripheral dose without compromising their effectiveness.

Low-intensity focused ultrasound (LiFUS) has been extensively studied in the last decade as a non-invasive tool to modulate BBB permeability and improve drug delivery. This technology, associated with intravenous (*i.v*) injection of microbubbles (MB), allows to create a cavitation phenomenon in contact of ultrasound (US) that disrupts the tight junctions between endothelial cells, leading to a transient BBB opening (BBBO) demonstrated in rodent models and even in humans[11-16]. It presents several advantages for the treatment of brain disorders, mainly its non-invasiveness, allowing for repeated treatments in the case of chronic diseases. Moreover, its spatio-temporal control allows to choose the right period and brain location of treatment. Importantly, LiFUS can be combined with different therapeutic agents without requiring any structural modifications to improve their brain delivery. The safety of LiFUS-BBBO has been extensively studied and is now well demonstrated in preclinical models, including mice, rabbits, sheep, nonhuman primates, and more recently in human clinical trials[38-43].

Interestingly, in the context of AD, LiFUS+MB demonstrated interest by itself as some studies in mouse models of the disease showed a decrease of amyloid plaques[17-21], and even the tauopathy[6,7,22]. LiFUS+MB could also restore the long-term potentiation (LTP) levels in the hippocampus, essential in memory processes[23]. Studies tend to show an upregulation of inflammatory processes after LiFUS+MB but the time course of this response is not consistent, and mechanisms involved not well understood.

Indeed, Rigollet et al., demonstrated recently that LiFUS+MB led first to microglial activation (1 day after LiFUS+MB) followed by an astrocytic response (day 2), both normalized 7 days post treatment[24], while other showed that the microglial response ended 24h after LiFUS+MB treatment whereas astrocyte reactivity was still persistent[25]. Another study observed an increase in microglial activation, accompanied by improvement of Aβ phagocytosis 3 days after chronic LiFUS+MB treatment[17]. Transcriptomic studies also confirmed the upregulation of neuroinflammatory processes at short term[26-28]. Interestingly, high doses of US (548 kHz) induced elevated levels of the glial fibrillary acidic protein (GFAP) and ionized calcium-binding adaptor molecule 1 (IBA1), markers upregulated in reactive astrocytes and microglia respectively, that persist 7 weeks after a single FUS exposure[29]. The same study also showed that a repeated exposure to FUS (6 weekly sonications) led to an upregulation of GFAP, IBA1 and cluster of differentiation 68 (CD68), another microglial marker overexpressed in neuroinflammatory conditions, 1 week after the last sonication, but authors did not investigate at longer timepoints post-FUS. Finally, another study demonstrated the importance of determining the right therapeutic window, engendering BBB opening without sterile inflammatory response[30]. This window depends on mechanical parameters of US administration and MB volume injection and may explain the discrepancy of results observed in the literature. Moreover, almost all studies on neuroinflammatory responses after LiFUS+MB focused on short term delays. Consequently, even if the safety of LiFUS+MB procedure is already investigated in human AD patients[16,31], it appears crucial to further understand their impact on brain functions and neuroinflammatory response, particularly after repeated exposures, necessary for chronic diseases' treatment.

In this study, we therefore used the TgF344-AD rat model of AD, developing amyloid plaques, neuroinflammation and at later stage an endogenous tauopathy[32], to investigate the effect of a single or multiple exposure to LiFUS+MB in the entire brain, on microglial response and amyloid load.

Material and methods

Animals. Male and female TgF344-AD (TgAD) rats carrying the human $APP_{swedish}$ and PS1dE9 transgenes on a Fisher 344 background[32] were housed with food and water *ad-libitum* in a 12-hours light-dark cycle. Three cohorts were used: 1) To validate the BBB opening in the entire brain, WT rats (15-19-month-old) received an intravenous (*i.v*) injection of the radiotracer [^{99m}Tc]diethylenetriamine-pentaacetate ([^{99m}Tc]DTPA, n=2) or Blue Evans (n=2) after a LiFUS+MB exposure. 2) To evaluate the acute impact of our LiFUS+MB procedure, TgAD rats received one LiFUS+MB treatment at 19-20-month-old (n=6/sex/group) and euthanized 24h later. Age- and sex- matched TgAD rats receiving no US (Sham) were used as control. 3) To evaluate the impact of repeated LiFUS+MB sessions, TgAD rats received 4 LiFUS+MB exposure once a week at 11-month-old (n=6/sex) and euthanized 6 weeks after the last treatment at 13-month-old. Control TgAD rats underwent anesthesia for 20 min each week (sham-treated animals; n=6 females, 2 males). 4) To evaluate the capability of LiFUS+MB to efficiently increase Adu antibody delivery into the rat brain, 20-month-old WT (n=2) and TgAD (n=2) were treated with LiFUS+MB followed by an *i.v* injection of [^{125}I]Adu and euthanized 24h later. Animals were randomly

assigned to groups. All experimental procedures were approved by the Ethics Committee for Animal Experimentation of the Canton of Geneva, Switzerland.

Low-intensity Focused Ultrasound treatment. The US setup featured a 7-element annular concave transducer (25 mm diameter, 20 mm radius of curvature, Imasonic, France) with a central frequency of 1.5 MHz. This transducer was driven by a 16-channels sine wave phased array, output power maximum 3W/channel, synchronized with a motorized XY stage (Image Guided Therapy (IGT), France) and associated to a degassing water circuit for removing air bubbles from the water-filled balloon. The XY motorized stage allows a synchronous transmission of FUS with transducer movement (BBBop software; IGT). Acoustic pressure delivery was measured using a 200-µm calibrated hydrophone (HGL-0200, preamplifier AH-2020, Onda Corporation, USA), mounted on a micrometric 3D positioning stage and placed at the transducer's focus in a water tank (Figure 1A). The -6 dB focal dimensions of the focal spot were 7 mm axially and 1 mm laterally. The acoustic transmission at 1.5 MHz through the male and female rat skulls were measured at different ages using experimental setups described by Gerstenmayer and collaborators[33] and taken into account to tune up the acoustic pressure to 450kPa at the focal point *in situ* (Figure 1B).

Under isoflurane anesthesia, the animals were shaved and positioned in a dedicated bed within a stereotactic frame. The transducer was coupled to the head using a latex balloon filled with deionized and degassed water, and acoustic gel was applied to the skin to ensure effective coupling with the balloon. A bolus of commercially available MB (400 µl/kg; SonoVue®, Bracco, Italy) was injected into the tail vein. US sonication started immediately after the MB injection, using continuous waves set to an estimated peak negative (PN) acoustic pressure of 450kPa in situ at the focus. One minute later, a second bolus of MB was administered (400 µl/kg, SonoVue). Amplitude compensation was applied according to the animal's weight and sex. For the two first cohorts, the transducer was moved back and forth over the posterior area of the rat brain (targeting the 2 hippocampus and cortex region above) along 6 axes, covering a surface of 12mm x 6mm at 2 different depths (steering position with a focal depth of 25 mm; Figure 1C). Pseudo-continuous US waves were transmitted for a total duration of 3.2 minutes[34]. For the third cohort, only the left hemisphere was sonicated in order to use the contralateral hemisphere as control. A surface of 10mm x 6mm was covered at two different depths.

Aducanumab radiolabeling. 120 µg of Adu (Selleckchem) was added to 10µl of [^{125}I]NaI (30 MBq, PerkinElmer) and diluted into PBS0.1M (100 µl final). Fifteen µl of Chloramine T (1g/ml) were then added and the mixture incubated for 90 sec before the addition of 15 µl of metabisulfites (2g/ml). After antibody radiolabeling, the total volume was completed at 500 µl with PBS0.1M. A purification step was realized on a NAP-5 column. Briefly, the column was rinsed with 10 ml of PBS0.1M and the solution containing the radiolabeled solution was passed through. The first fraction corresponds to the void fraction. Then, 1ml of PBS0.1M was added to the column to obtain the high molecular weight fraction, containing the radiolabeled antibody. Finally, 2x750 µl of PBS0.1 allow to eluate the low molecular weight fraction containing free iodine. After an evaporation step, [^{125}I]Adu was resuspended into saline solution before injection.

SPECT imaging. For [^{99m}Tc]DTPA imaging, rats (n=2) were anesthetized (3% isoflurane) and were placed in the U-SPECT-II scanner (MiLabs). They received a tail-vein injection of the radiotracer [^{99m}Tc]DTPA (50 MBq) and a 30min SPECT scan was acquired 30 min after injection. Animals were immediately euthanized after SPECT imaging.

For [^{125}I]Adu, the radiolabeled antibody was injected into the tail vein of the animal (23,3 MBq/rat) of the fourth cohort under isoflurane anesthesia, 5min after the LiFUS+MB exposure. At T+3h and T+24h after the injection, the animal was placed in the U-SPECT-II scan (MiLabs) and a 30min SPECT scan was acquired. Animals were immediately euthanized after the last SPECT scan.

SPECT images were reconstructed using a P-OSEM (0.4 mm voxels, 4 iterations, 6 subsets) method with a radioactive decay correction. Images were manually co-registered to the T2 Schiffer template on PMOD software (version 4.4, PMOD Technologies Ltd).

***Ex vivo* autoradiography.** Frozen brains from SPECT-scanned rats were cryosectioned into 25 µm coronal sections. Sections from each animal were immediately exposed to a phosphor imaging plate (BAS 1800II - Fujifilm) overnight (O/N). The resulting digital images were analyzed with the AIDA image analysis software (Elysia-Raytest). The same sections were then stained with methoxy-X04 (MX04, 20 µg/ml; Tocris) in PBS0.1M for 30 min at RT to label amyloid plaques.

Evans blue. An Evans blue 4% (2 ml/Kg) solution was injected in the tail vein of animals (n=2), 5 min after the LiFUS+MB sequence. The animal was euthanized by an injection of pentobarbital 60 min later. The brain was then dissected in 1mm slices in a brain matrix to assess the surface and depth of the BBB opening.

Histology. 24h after the LiFUS+MB treatment (cohort 2), TgAD rats were killed under anesthesia (2% isoflurane) by intracardiac perfusion with a saline solution. One hemisphere was postfixed in a 4% paraformaldehyde solution for 24h and cryoprotected with a sucrose gradient (10 to 20%) before being frozen in isopentane. Serial brain sections (35 µm) were realized with a cryostat and stored in an anti-freeze solution at -20°C until used for histology. The other hemisphere was rapidly dissected to isolate the hippocampus and surrounding cortex and snap frozen in liquid nitrogen for RT-qPCR measures.

After washes in PBS0.1M, slices were mounted on slides and let dry O/N. Slices were rehydrated in PBS0.1M and incubated O/N at 4°C with the following primary antibodies: anti-GFAP-Cy3 (1/1000, Mouse; Sigma) or anti-IBA1 (1/500, Rabbit; Wako) in 1% BSA/PBS0.1M/0.3% Triton X-100. After 3 washes in PBS0.1M, slices were incubated for 1h at room temperature in the appropriate secondary antibody (1/250, Alexa Fluor) in 1% BSA/PBS0.1M/0.3% Triton X-100. Finally, slices were rinsed before being coverslipped with Fluorosave™ (Calbiochem).

Histological image analysis. Images were acquired at 10x magnification using the Axioscan.Z1 scanner (Zeiss) and analyzed with the QuPath software[35]. The hippocampus and the surrounding cortex were manually delineated. An intensity threshold, consistent across all subregions, was applied to quantify the percentage of the region of interest (ROI) that was positively stained with GFAP, or IBA1.

Protein extraction. For the cohort 3, animals were euthanized under anesthesia (2% isoflurane) by intracardiac perfusion with a saline solution. Both hemispheres were dissected to collect the hippocampus and the adjacent cortex for biochemistry or flow cytometry (see details below). Proteins were extracted in a Triton X100 lysis buffer [50 mM Tris-HCl pH = 7.4, 150 mM NaCl, 1% Triton X-100 with 1x protease and phosphatase inhibitors (Pierce); 500 µl], centrifuged at 20,000 g for 20 min at 4 °C. The supernatant contains Triton X100 (Tx)-soluble proteins. The pellet was re-suspended in a Guanidine lysis buffer [50 mM Tris-HCl pH = 8, 5 M Guanidine HCl with 1x protease and phosphatase inhibitors (Pierce); 250 µl], incubated for 3h on ice and centrifuged at 20,000 g for 20 min at 4 °C. The supernatant contains Guanidine (Gua)-soluble proteins. The total protein concentration was determined using the BCA test (Pierce).

ELISA tests. Aβ peptides were measured using the human Aβ40 ELISA test (Life Technologies) and human Aβ42 ELISA test (Life Technologies). Tx-soluble samples were diluted at 1/10 (females), 1/50 (males) in the diluent buffer provide in $A\beta_{40}$ kit, and at 1/250 (females and males) in the diluent buffer for $A\beta_{42}$. Gua-soluble samples were diluted at 1/100 (females), 1/600 (males) in guanidine buffer and then at 1/500 in diluent buffer for $A\beta_{40}$; 1/600 (females and males) in guanidine buffer and then at 1/500 in diluent buffer for $A\beta_{42}$. Manufacturer's protocols were followed. Absorbances were measured at 450 nm using the SpectraMax iD3 plate reader (Molecular devices). The absence of amyloid in WT was validated for all forms. Aβ concentrations were determined using a 4S parameters analysis and were normalized to the total protein quantity (µg proteins).

[^{125}I]CLINDE synthesis. The CLINDE tributyltin precursor (100 µg) was resuspended in 10µl of Hexafluoro-2-propanol (HFIP). The precursor was then incubated with 3mg of Sodium acetate, 95µl of N-Chlorosuccinimide (at 0.016M in HFIP) and 10µl of [^{125}I]NaI (10MBq, PerkinElmer) for 25 min at RT. Reactions were then diluted in 50% acetonitrile (ACN) in water (350µl), injected onto a reversed-phase column (Bondclone C18) and [^{125}I]CLINDE, a TSPO specific radiotracer, was isolated by a linear gradient HPLC run (5% to 95% ACN in 7mM H3PO4, 10 min). At the end, ACN was evaporated and [^{125}I]CLINDE was dissolved in saline.

Cell dissociation. Hippocampal and cortical tissues were collected in cold HBSS before a mechanical and enzymatic dissociation followed by a myelin depletion step (Miltenyi biotec). Cells were then suspended in 0.1 M PBS/ 1 mM EDTA/ 1% of BSA buffer and incubated with [^{125}I]CLINDE (1.4MBq/sample) for 15 min on ice. After a washing step, cells were treated with an anti-rat CD32 (1/100; BD Bioscience) for 5 min on ice to block Fc-mediated adherence of antibodies. After a centrifugation at 350 g, 5 min at 4°C, cells were resuspended with a solution of the primary antibody, PerCP/Cyanine5.5 anti-rat CD11b/c (1/100; 201820, Biolegend), diluted in 0.1 M PBS/ 1 mM EDTA/ 1% of BSA buffer for 20 min on ice. After washing and centrifugation at 350 g, 5 min at 4°C steps, cells were suspended in 400 µl of 0.1 M PBS for cell sorting.

Fluorescence activated cell sorting. Unstained and single stain cells were used to identify positive and negative cells for each antibody, to identify auto-fluorescent cells, to determine the values of compensation (to correct for interference between fluorochromes) and to draw sorting gates for each antibody. Cells were first sorted based on their forward and side scatter from all detected events. Dead

cells were excluded using DAPI staining before cell sorting. Microglia cells were sorted based on their fluorescence for PerCP/Cy5.5-CD11b. Cell numbers were determined during cell sorting on a BD FACSAria™ Fusion Flow Cytometer (BD Biosciences),

***Ex-vivo* radioactivity counting**. Radioactive concentrations in sorted microglia were measured on an automatic γ counting system (Wizard 3", PerkinElmer). Data are expressed in count per minute (CPM)/g of tissue or CPM/number of cells for each animal.

RNA extraction and qPCR. Samples (sorted cells or tissue homogenates) were placed into 400 µl of Trizol before storage at -80°C. The day of the extraction, samples were left at RT for 5 min. Then, 100 µl of chloroform was added for 3 min. After a vortex and centrifugation at 12,000 g for 15 min at 4°C, the aqueous phase was collected and 1 volume of ethanol 70% was added. The whole volume was then transferred onto RNeasy columns (RNeasy micro kit, Qiagen) and the manufacturer's protocol was followed. RNA was eluted with 15 µl of nuclease free water. Superscript IV VILO synthesis kit (Invitrogen) was used to synthesized cDNA as described by the manufacturer. Samples were diluted at 1/10 in H_2O and mixed with 250 nM of primers and PowerUp SYBR Green Master Mix (Applied Biosystems) for qPCR. The following sequences of primers were used: *Aif1-F:* CAGAGCAAGGATTTGCAGGGA*, Aif1-R:* CAAACTCCATGTACTTCGTCTTG*; ApoE-F: CTGAACCGCTTCTGGGATTACCTG; ApoE-R: CATAGTGTCCTCCATCAGTGCCGTC; C3-F: GACCTGCGACTGCCCTACTCT, C3-R: CTGATGAAGTGGTTGAAGACG; Clusterin-F:* AGCGCACTGGAGCCAAG, *Clusterin-R:* TCAGAGACCTCCTGCTCTCC; *Cx3cr1-F:* TCTTCACGTTCGGTCTGGTG*, Cx3cr1-R:* GGCAAAGTGGCCACAAAGAG*; Gfap-F: TTGACCTGCGACCTTGAGTC, Gfap-R: GAGTGCCTCCTGGTAACTCG; Glut1-F:* GCATCTTCGAGAAGGCAGGT*, Glut1-R:* AACAGCGACACCACAGTGAA*; Il1β-F:* CACACTAGCAGGTCGTCATCATC, *Il1β-R:* ATGAGAGCATCCAGCTTCAAATC; *Il4-F:* AGACGTCCTTACGGCAACAA, *Il4-R:* CACCGAGAACCCCAGACTTG; *Il6-F:* AGAGACTTCCAGCCAGTTGC, *Il6-R:* AGTCTCCTCTCCGGACTTGT; *Itgam-F:* CTTGGTGAAACCCGAGTGGT, *Itgam-R:* TCGATCGTGTTGATGCTACCG*; Mbp-F:* TCTCAGACCGCCTCAGAAGA*, Mcu-F: ACAGTTTGGCATTTTGGCCC, Mcu-R: ATTCCTGGCGCGTCATTACA; Mbp-R:* TGTGCTTGGAGTCTGTCACC*; Mct1-F:* GCTGCTTCTGTTGTTGCGAA*, Mct1-R:* AAATCCAAAGACTCCCGCGT*; Mct4-F:* CGATACTTCAACAAGCGCCG, *Mct4-R:* CAGTGCACAAAGGAACACGG*; NeuN-F:* GAGTCTATGCGGCTGCTGAT, *NeuN-R:* CAGAGGCTAGCCATGGTTCC*; Ppia-F:* ATGGCAAATGCTGGACCAAA, *Ppia-R:* GCCTTCTTTCACCTTCCCAAA; *P2y12r-F:* AACGCCTGCCTTGATCCATT*, P2y12r-R:* TACATTGGGGTCTCCTCGCT*; Rantes-F: GCAGTCGTCTTTGTCACTCG, Rantes-R: GGAGTAGGGGGTTGCTCAGT; Stat3-F:* CAACTTCAGACCCGCCAACA, *Stat3-R:* GCCGCTCCACCACGAAGG; *Tgfβ-F:* CCTGGAAAGGGCTCAACAC, *Tgfβ-R:* CAGTTCTTCTCTGTGGAGCTGA; *Tnfα-F:* CAGAGCAATGACTCCAAAGTA, *Tnfα-R:* CAAGAGCCCTTGCCCTAA*; Trem2-F:* CCTGTGGGTCACCTCTAACC*, Trem-R:* GGCCAGGAGGAGAAGAATGG; *Tspo-F:* GCTGCCCGCTTGCTGTATCCT*, Tspo-R:* CCCTCGCCGACCAGAGTTATCA*; Vdac1-F:* GTCACCGCCTCCGAGAACAT*, Vdac1-R:*

CGTAGCCCTTGGTGAAGACA; *Vimentin-F*: CAGTCACTCACCTGCGAAGT, *Vimentin-R*: AGTTAGCAGCTTCAAGGGCA. Expression levels of genes of interest were normalized to the abundance of *Ppia* gene with the ΔCt method.

Statistics. Analyses were performed in blind conditions and normality of residues was assessed with the Shapiro-Wilks test. An unpaired *t*-test was performed if the normality conditions were respected, otherwise, a Mann-Whitney test was performed. Outliers were identified using the ROUT method (Maximal false discovery rate = 1%). All analyses were performed on GraphPad Prism 10. Statistical details are provided only if significance was reached.

Results

Calibration of Experimental apparatus for LiFUS+MB treatment

Multiple studies described a safe BBB opening in rodents with an *in situ* peak negative acoustic pressure set at 450 kPa[30,36]. Consequently, we first calibrated our LiFUS apparatus in degassed water using a hydrophone to determine the amplitude necessary to reach a maximum of 450 kPa at the natural focal point (focal depth at 20 mm) or at the steering point (focal depth at 25 mm) (Figure 1A and Supplemental figure 1). The impact of skull thickness on US transmission was also measured in our TgAD rat model. As sex and age are two factors influencing skull thickness, the coefficient of transmission (%) of US through the skull was measured for males and females at different ages (6, 10, 16, and 25-month-old; Figure 1B). It is important to note that animals begin to lose weight after a certain age. Therefore, considering the age of the animals rather than their weight appears more relevant, particularly when using aged animal models for studying degenerative diseases. Once LiFUS parameters were determined to reproducibly apply an acoustic pressure of 450 kPa, we developed a sequence to target the entire rat brain (Figure 1C). We validated the efficient BBB opening by SPECT imaging using [^{99m}Tc]DTPA (Figure 1D) or an intravenous injection of Evans blue (Figure 1E), which only penetrate the brain in the presence of an alteration of the BBB.

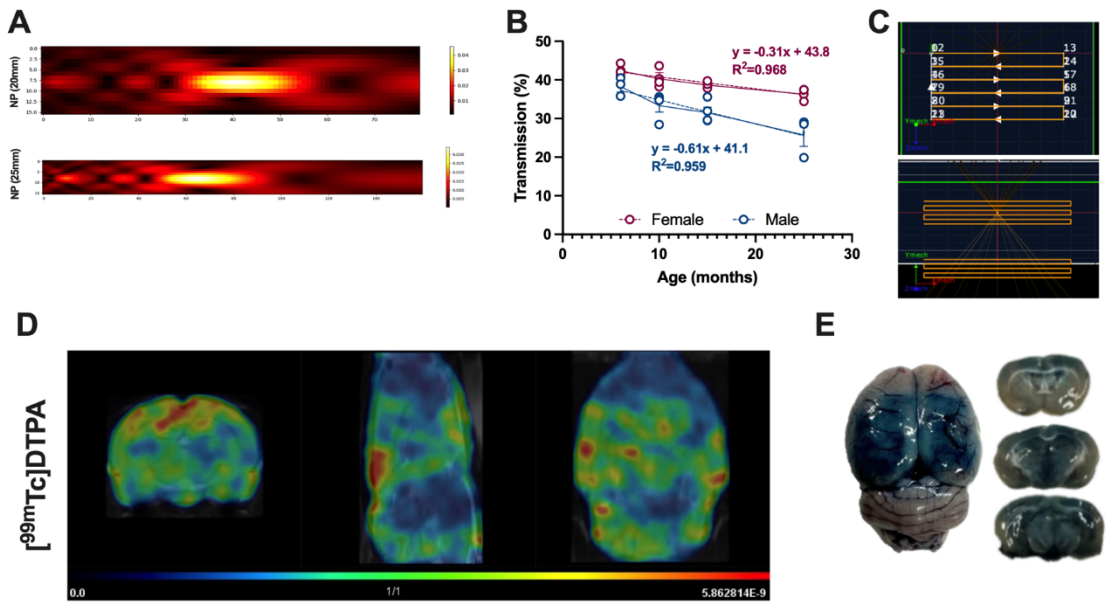

Figure 1: Experimental apparatus for LiFUS+MB treatment and efficient BBB opening in rats.

A) To calibrate our apparatus for LiFUS+MB treatment, a submersible hydrophone was placed in degassed water below the transducer. The measurement of the peak negative acoustic pressure delivered by the transducer was realized at 20 (natural point) and 25 mm (steering). **B)** The coefficient of transmission through the skull was determined depending on the age and the sex of WT rats. **C)** A sequence with two focal points (natural focal point and steering point) was developed to target the entire rat brain. **D, E)** [^{99m}Tc]DTPA signal acquired by SPECT imaging **(D)** and Evans blue **(E)** staining in a female brain after LiFUS+MB treatment validating the BBB opening in the entire brain.

Impact of a single LiFUS+MB exposure on neuroinflammation

We then investigate the impact of a single LiFUS+MB exposure on neuroinflammation markers at an advanced stage of the pathology. The percentage of IBA1$^+$ area was unchanged in hippocampal subregions and in the surrounding cortex 24h after LiFUS exposure (Figures 2A-C). In the same way, the percentage of GFAP$^+$ area was not modified in the treated group (Figures 2D-F). To go further, we measured the mRNA expression of several glial and inflammatory markers in the brain (hippocampus and surrounding cortex) of sham- and LiFUS+MB-treated rats. Among microglial gene expression quantified, *Aif1*, the gene encoded IBA1, was overexpressed 24h after LiFUS (p=0.0125*;* Figure 2G). Moreover, an upregulation of *Gfap* (p=0.0440) and *Vimentin* (p=0.0109) mRNA levels, specifically expressed by astrocytes, suggested that astrocyte reactivity is induced by a single sonication (Figure 2H). Other microglial and astrocytic gene expression were unchanged (Figure 2G, H). To deepen characterize the inflammatory response at the transcriptional level, we quantified the expression of pro- and anti-inflammatory gene levels (Figure 2D). The 18kDa translocator protein (TSPO) is a classical marker of neuroinflammation known to be overexpressed in glial cells of animal models and AD patients' brain, even before the appearance of classical neurochemical markers and cognitive symptoms of AD[37-40]. Interestingly, an increase in *Tspo* mRNA levels was measured after LiFUS+MB (p=0.0002), (Figure 2I). Furthermore, the interleukin 6 *(Il6; p*=0.0041*)* and chemokine *Rantes* (p=0.0140) gene expression

were upregulated in LiFUS+MB-treated group compared to sham-treated animals whereas, surprisingly, the tumor necrosis factor α (*Tnfα; p*=0.0415) was downregulated (Figure 2I). These changes suggest a global inflammatory response to a single LiFUS+MB exposure 24h post-treatment. Other mRNA levels (transforming growth factor beta (*Tgfβ*), nuclear factor-kappa B (*NFκB*), the interleukins Il1β and *Il4*, *complement C3*) were unchanged (Figure 2I). No difference between males and females was observed.

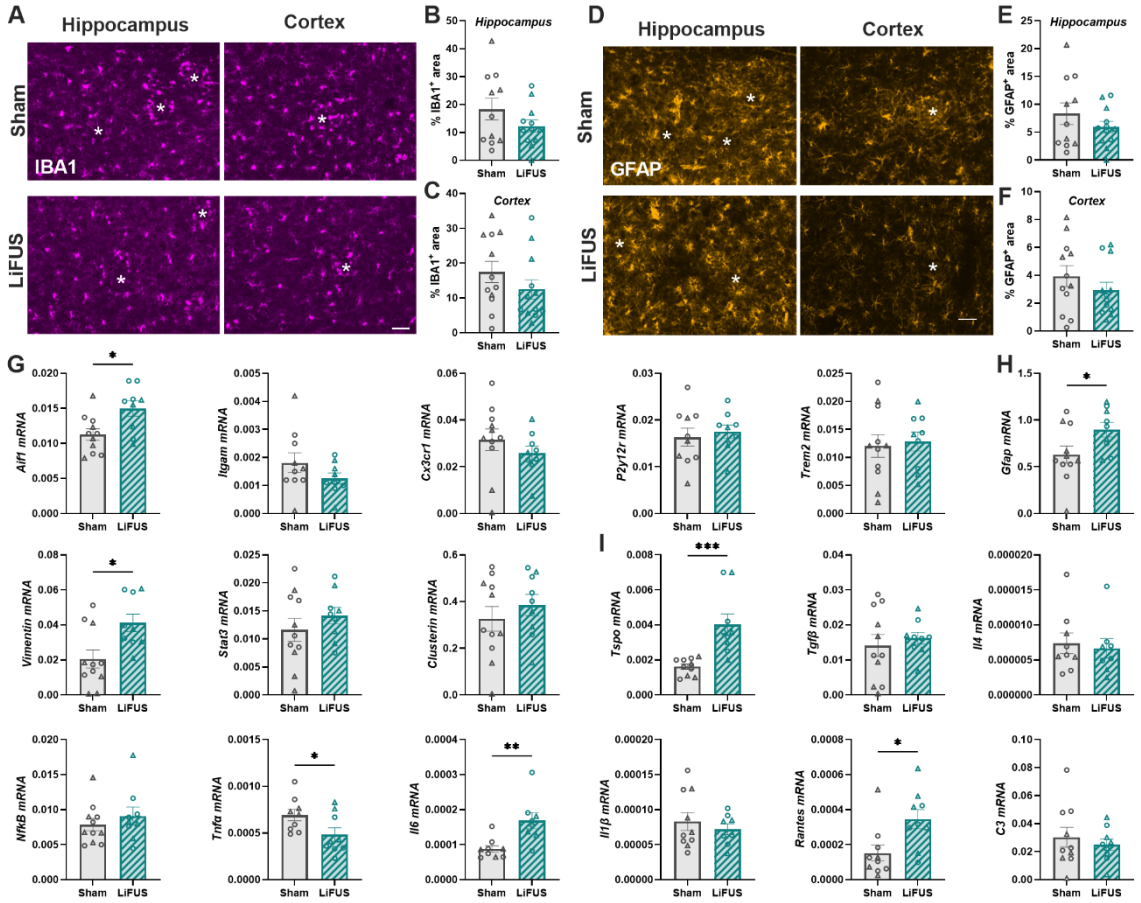

Figure 2: A single LiFUS+MB exposure slighlty modulates astrocyte and microglial reactivity 24h post-treatment in TgAD rats.

A-C) Representative images of IBA1 (magenta; **A**), a microglial marker, in the hippocampus and the cortex of sham-treated TgAD rats and LiFUS+MB-treated TgAD rats. Quantification of the % IBA1$^+$ area **(B, C)** in both regions. **D-F)** Representative images of GFAP (orange, **D**), an astrocytic marker, in the hippocampus and the cortex of sham-treated TgAD rats and LiFUS+MB-treated TgAD rats. Quantification of the % GFAP$^+$ area **(E, F)** in both regions. Stars represent amyloid plaque localization. Scale bar = 50 µm. **G-I)** mRNA levels of microglial (**G**), astrocytic (**H**) and inflammatory (**I**) genes in the hippocampus and surrounding cortex homogenate in sham vs LiFUS+MB-treated groups. Unpaired student *t* test and Mann-Whitney test. *p≤0.05, **p≤0.01, ***p≤0.001. Males are represented by round points and females by triangles.

Persistent effect of repeated LiFUS+MB exposure

Microglia are known to be the main producers of inflammatory cytokines in the brain[41-43] and are highly adaptive cells that respond functionally to changes in their environment, such as exposure to FUS[44]. Consequently, in a second cohort, we investigated the effect of repeated LiFUS+MB treatment on neuroinflammation, with a focus on microglial cells and amyloid load in pre-symptomatic TgAD rats of 13-months-old. The effect of repeated LiFUS treatment was measured at the cellular level on sorted microglia ($CD11b^+$) from hippocampus and cortex region of sham-treated and LiFUS+MB-treated TgAD rat brain. Sorted cells expressed genes known as microglia markers (*Itgam*, *Aif1* and *Cx3cr1*) whereas they did not express markers of other cell types (*Gfap*, astrocytes; *Neun*, neurons; *Mbp*, oligodendrocytes), validating the efficient sorting of microglia (Figure 3A). The LiFUS+MB treatment did not impact the expression of cell type markers and the proportion of sorted microglia (Figure 3A, B).

We first investigated the inflammatory state of microglia by measuring *in vitro* in sorted cells the binding of [^{125}I]CLINDE, a radioligand of TSPO. Interestingly, we observed a decrease in TSPO levels in the total parenchyma cell population before cell sorting ($p=0.0314$; Figure 3C), as well as a reduction in TSPO levels per microglia ($p<0.0001$; Figure 3C) in LiFUS+MB-treated rats. This suggests that TSPO downregulation in microglia could explain in part the total downregulation of TSPO after repeated LiFUS treatment. We then validated this decrease in microglia at the mRNA level ($p=0.0453$), which was accompanied by an increase expression of *Tnfα* ($p=0.0049$) and *Tgfβ* ($p=0.0193$), a pro- and an anti-inflammatory marker respectively (Figure 3D). Moreover, a decrease of the expression of the *Purinergic receptor P2Y G-protein coupled 12* (*P2y12r*) gene was observed after LiFUS+MB treatment (Figure 3D). P2Y12R is described as one of the most specific microglia markers and a loss of its expression in microglia has been reported to be associated with pro-inflammatory microglia in several diseases linked to neuroinflammation, such as AD[45,46]. No changes in the mRNA expression of the receptor TREM2 and the C3 complement protein were observed (Figure 3D). Overall, a repeated treatment of LiFUS+MB modified the inflammatory status of microglia.

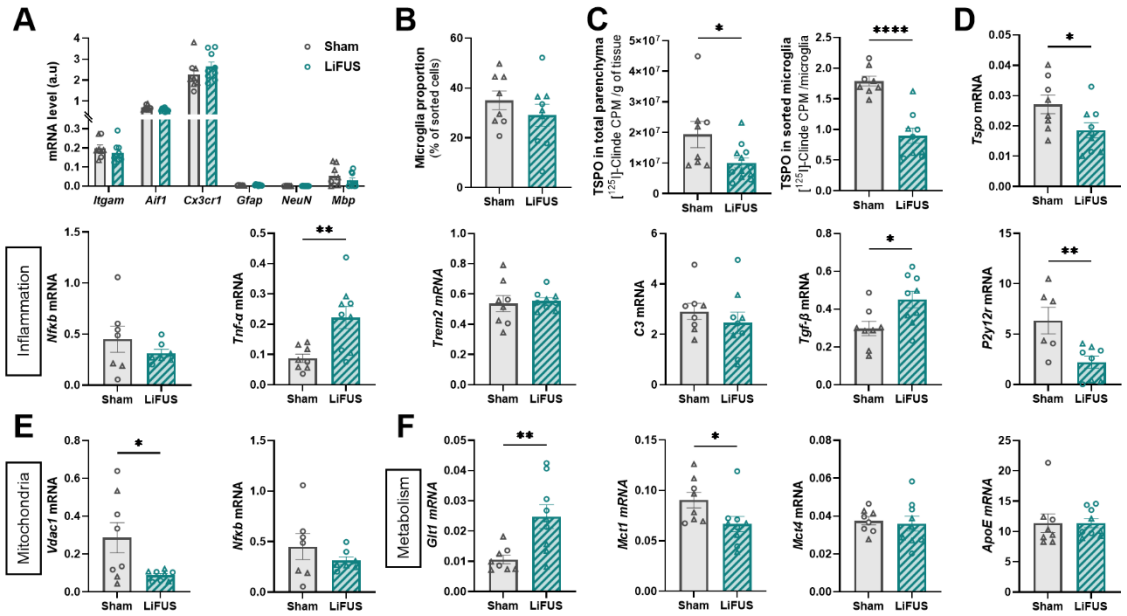

Figure 3: Repeated LiFUS+MB exposures impact microglial functions 6 weeks post-treatment in TgAD rats. **A)** Sorted cells expressed microglia genes (*Itgam*, *Aif1* and *Cx3cr1*) but did not express astrocyte (*Gfap*), neuron (*NeuN*) and oligodendrocyte (*Mbp*) specific genes. **B)** The percentage of sorted microglia was not modified by LiFUS+MB treatment. **C)** *In vitro* quantification of [^{125}I]CLINDE binding (count per minute, CPM), a TSPO radioligand. TSPO levels were decreased in total parenchyma (hippocampus+ cortex) and in sorted microglial cells after a repeated treatment of LiFUS+MB. The mRNA expression of different markers of inflammation (**D**), mitochondria (**E**) and metabolism (**F**) in microglia was modified by repeated LiFUS+MB treatment**.** Unpaired student *t* test. *p≤0.05, **p≤0.01, ***p≤0.001, ****p≤0.0001. Males are represented by round points and females by triangles.

To better understand the changes induced by a repeated LiFUS+MB treatment on microglia profile, we explored other important microglial functions. As TSPO is expressed in the outer mitochondrial membrane, we first measured the expression of genes involved in mitochondrial functions (Figure 3E). A decrease in the mRNA level of the voltage dependent anion channel 1 (*Vdac1*) was observed in the microglia of LiFUS+MB-treated TgAD rats compared to the sham-treated group (p=0.0264, Figure 3E). Another important cell function known to be impacted in AD is the metabolism, notably in microglia cells[47]. After repeated LiFUS+MB exposure, we observed an increase of glucose transporter 1 (*Glut1*) expression in sorted microglia (p=0.0053, Figure 3F). On the contrary, the mRNA level of the monocarboxylate transporter-1 (*Mct1*), playing a role in the lactate and ketone bodies transport, was decreased in microglia of the LiFUS+MB-treated group (p=0.0462, Figure 3F). No difference in the mRNA expression of *Mct4* and *ApoE*, involved in lipid metabolism, has been measured after the LiFUS treatment (Figure 3F). These results showed that the modification of the inflammatory state of microglia observed following repeated LiFUS+MB treatment was associated with changes in the expression of genes involved in key microglia functions in the context of AD.

To determine if those changes in microglial functions, known to play a key role in Aβ removal, influenced Aβ load, we quantified different Aβ peptides and aggregation forms by ELISA. In our conditions, repeated LiFUS+MB did not modulate the soluble or poorly aggregated forms of Aβ40 and Aβ42 (Figure 4A) nor the highly aggregated forms (Figure 4B).

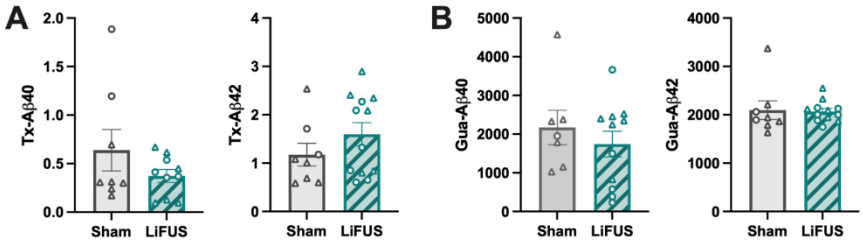

Figure 4: Repeated LiFUS+MB exposures did not impact amyloid load 6 weeks post-treatment in TgAD rats. Triton (Tx)-soluble **(A)** and Guanidine (Gua)-soluble **(B)** forms of Aβ40 and Aβ42 were measured by ELISA in the hippocampus + adjacent part of the cortex in sham-treated TgAD rats and TgAD rats treated 4 times once per week with LiFUS+MB. Unpaired student *t* test or Mann-Whitney test. Males are represented by round points, females by triangles.

As LiFUS+MB did not decrease Aβ pathology by itself in our AD rat model, we assessed the capacity of our LiFUS+MB protocol to increase the brain delivery of one of anti-amyloid antibody recently approved by FDA. In a proof-of-concept experiment, we therefore treated our rat model with LiFUS+MB following with an *i.v* injection of the radiolabeled [^{125}I]Adu antibody. We then followed the entry and accumulation of [^{125}I]Adu into the rat brain with SPECT imaging 3h and 24h post-treatment and observed a high SPECT signal in the LiFUS-treated hemisphere compared to the contralateral side in the Tg-AD rats at both time-points (Figure 5A), suggesting an increase of the antibody brain penetration with LiFUS+MB pre-treatment. The difference of signal level between TgAD and WT rats validated the specificity of the [^{125}I]Adu signal (Figure 5A). Finally, the binding specificity of the antibody was confirmed with an *ex vivo* autoradiography (Figure 5B) and an immunostaining of amyloid plaques (Figure 5C).

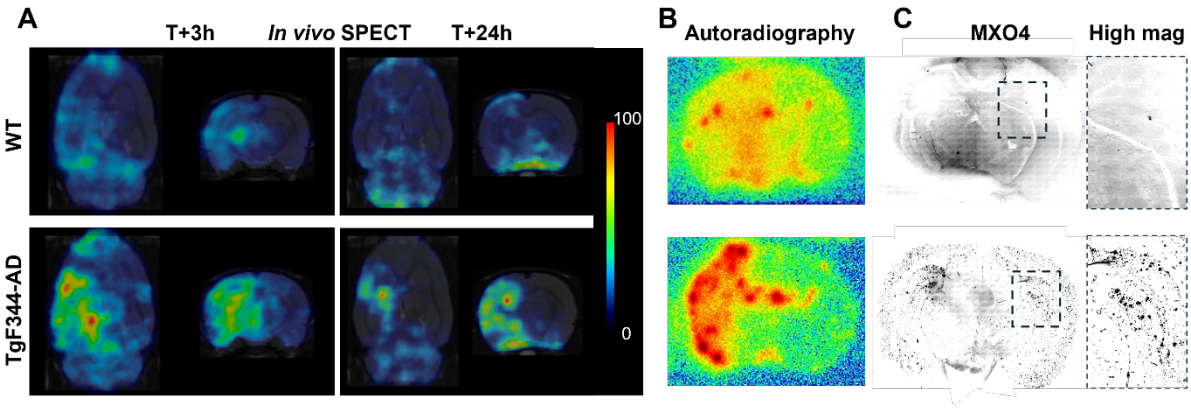

Figure 5: **LiFUS treatment improves anti-Aβ antibody brain delivery**

[^{125}I]Adu-SPECT imaging (**A**) were acquired 3h and 24h after LiFUS+MB treatment of the left hemisphere of WT and TgAD rats. The accumulation of radiolabeled Adu in the targeted hemisphere demonstrated the ability of LiFUS+MB-mediated BBB opening to improve Adu delivery in rat brain. The very low signal observed in the brain

of WT animal compared to the TgAD rat validated the specific binding in our model, as confirmed by *ex vivo* autoradiography **(B)** and Aβ plaques staining (MX04, black points, **C**).

Discussion

For the development of our LiFUS+MB experimental procedure, the measure of skull thickness demonstrated a clear difference between sex, and age. Both parameters are essential to consider when setting up the experimental conditions for LiFUS exposure. Moreover, the age appears more relevant than weight, particularly when working with old animals, as animals lose weight after a certain age. With the adjustment of our LiFUS+MB protocol based on sex and age, our results showed that the treatment did not affect male and female rats differently.

To investigate the impact of a single exposure to LiFUS+MB on neuroinflammation, the entire brain of TgAD rats was treated and analyzed 24h post-treatment. Interestingly, we observed that a single session of LiFUS+MB led to an overexpression of inflammatory genes including *Aif1* (microglia specific), *Gfap* and *Vimentin* (astrocyte specific), *Tspo, Il6* and *Rantes* (pro-inflammatory molecules) 24h after treatment. Surprisingly, a decrease expression of *Tnfα* accompanied with no change in *Nfκb* level were measured, suggesting that the TNFα/NFκB pathway does not seem to be involved in the inflammatory response observed 24h after a single treatment in our conditions. However, any change was observed at the protein levels when we quantified the % area positively stained for IBA1 or GFAP. It would be interesting to measure those markers at shorter or longer timepoints to better determine the dynamic of the inflammatory response after our protocol. Indeed, the majority of studies tends to agree on a pro-inflammatory effect of LiFUS+MB but the time course of microglial and astrocyte reactivity diverge between studies[17,24,26-29]. Moreover, we cannot also exclude that the neuroinflammatory response is too slight to be visible at the protein level using immunohistochemistry in our experimental conditions. Consequently, it would be interesting to validate these results using more sensitive and comprehensive proteomic approaches.

We then investigated the effect of a repeated LiFUS+MB treatment, 4 weekly sonications, with a particular interest on persistent effects. Brains were consequently analyzed 6 weeks after the last sonication. Our results showed a modulation of microglia phenotype after a repeated LiFUS treatment with changes in the mRNA expression of several inflammatory markers, both pro- (e.g. *Tnfα*, *Tspo*) and anti-inflammatory (e.g. *Tgfβ*). In recent years, the classification of activated microglia into two distinct categories, pro- and anti-inflammatory, has become increasingly debated. Instead, it is now described as a continuum of transformation, with microglia continuously adapting to their environment and monitoring it through ongoing morphological and functional changes[48]. In our conditions, after a repeated LiFUS+MB treatment, we observed a decrease in the expression of *P2y12r*, a specific microglia marker that is expressed in their processes interacting with astrocytic endfeet, pericytes and a part of the endothelial cells in cortical blood vessels[49]. A modulation of the *P2y12r* expression is therefore consistent with our LiFUS+MB procedure to open the BBB. Moreover, it has been shown that a low level of P2Y12R in microglia would be a marker of inflammatory around Aβ plaques in human brain[46,50].

Surprisingly, changes in TSPO density were also observed but unlike the single LiFUS+MB exposure, repeated treatment resulted in a reduction of TSPO at both the mRNA and protein levels, which was accompanied by an increase in *Tnfα* mRNA levels, a downstream modulator of the NFκB pathway. This upregulation has already been observed in cultures of TSPO-deficient human microglia and a compensatory mechanism was proposed in favor of the NFκB pathway, which would additionally be negatively regulated by TSPO[51,52]. The discrepancy in TSPO changes between single and multiple exposures would suggest that the TSPO level difference in repeated treatment was more associated with a functional adaptation of the microglia.

Indeed, in addition to the inflammatory changes, we showed modifications in the expression of genes involved in microglia key functions after a repeated LiFUS treatment. We notably measured a decreased expression of the mitochondrial gene, *Vdac1*. In recent years, a structural and functional interaction between VDAC1 and TSPO has been proposed and a reduction of the VDAC1 protein level is observed in TSPO-deficient human microglia culture which affected the intracellular Ca^{2+} homeostasis, important for the bioenergetic function of the cells[51,53]. Moreover, the slight changes in the inflammatory state of microglia after multiple LiFUS+MB exposure is also associated with a metabolic adaptation, with an upregulation of the glucose transporter *Glut1* gene expression, suggesting an increase of glucose uptake which may induce an upregulation of the glycolysis by microglia. Moreover, our result also showed a decrease of *Mct1* mRNA level without significative changes of the *Mct4*. MCT1 and MCT4 are both involved in the transport of lactate and ketone bodies but differ in substrate affinity and are preferentially implicated in lactate import for MCT1 and export for MCT4[54,55]. Our results would therefore suggest a metabolic shift in microglia after multiple exposure in favor of the glycolysis process compared to the anaerobic and ketolysis pathways, already described in inflammatory conditions[56-58].

In addition to inflammation modulation, different studies in mouse models of AD described a reduction of amyloid plaques after LiFUS exposure alone[17-19,21,59-62]. For the first time to our knowledge, we investigated the effect of LiFUS+MB on different poorly or highly aggregated forms of Aβ. Surprisingly, multiple exposures (4 weekly sonications) did not modulate soluble/poorly aggregated forms of $A\beta_{40}$ and $A\beta_{42}$ nor the highly aggregated forms of those peptides. Consequently, in our experimental conditions (LiFUS parameters, MB concentration, delay post sonication), by opening safely the BBB, LiFUS appears more promising as a key tool to improve drug delivery into the brain, allowing to reduce the i.v injected dose and reducing potentially the risk of side effects.

Research for AD therapies has known a renewal with the approval of three anti-amyloid immunotherapies by the FDA, and results from other immunotherapies targeting inflammation and tau are encouraging. Nevertheless, even if those therapies offer new exciting promises for patients, they are still associated with important adverse effects including amyloid-related imaging abnormalities (ARIA) resulting in cerebral edema and hemorrhages. The mechanisms leading to those side effects are not yet identified but could be related to the high dosage infused intravenously required to induce therapeutic outcomes[8,9,63]. The ability to LiFUS+MB to increase antibodies delivery has been increasingly studied in mouse model of AD[64-69] but, to our knowledge, this procedure has not been validated in the TgAD rat model, that present the advantage to harbor only amyloid mutations while

developing endogenous tauopathy, associated with neuroinflammation and cognitive alterations. In our proof-of-concept experiment, we validated that LiFUS was also efficient to improve the entry of the anti-amyloid antibody Adu into the rat brain. Further studies are necessary to investigate the benefit of antibody injected dose reduction through LiFUS on immunotherapy adverse effects such as ARIA, the synergic effects of LiFUS+MB and immunotherapies and the mechanisms involved in Aβ clearance.

Conclusion

Microglia are highly plastic cells capable of altering their phenotype and functions in response to environmental stimuli. Single LiFUS exposure induced a slight increase of astrocytic and microglial reactivity at the transcriptional level 24h post-treatment in our experimental conditions. Repeated LiFUS treatment seems to induce microglial reprogramming, leading to the adaptation of gene expression related to key functions such as inflammatory response, mitochondrial and energetic metabolism. Overall, LiFUS treatment did not induce major changes in AD pathological hallmarks but additional studies at other timepoints appear essential to better characterize their impact on neural cells and brain functioning in general. Finally, LiFUS+MB offers promising results when combined to Aducanumab antibody.

References

1 Escartin, C. *et al.* Reactive astrocyte nomenclature, definitions, and future directions. *Nat Neurosci* **24**, 312-325 (2021).

2 Miao, J. *et al.* Microglia in Alzheimer's disease: pathogenesis, mechanisms, and therapeutic potentials. *Front Aging Neurosci* **15**, 1201982 (2023).

3 Soderberg, L. *et al.* Lecanemab, Aducanumab, and Gantenerumab - Binding Profiles to Different Forms of Amyloid-Beta Might Explain Efficacy and Side Effects in Clinical Trials for Alzheimer's Disease. *Neurotherapeutics* **20**, 195-206 (2023).

4 Linse, S. *et al.* Kinetic fingerprints differentiate the mechanisms of action of anti-Abeta antibodies. *Nat Struct Mol Biol* **27**, 1125-1133 (2020).

5 Yadollahikhales, G. & Rojas, J. C. Anti-Amyloid Immunotherapies for Alzheimer's Disease: A 2023 Clinical Update. *Neurotherapeutics* **20**, 914-931 (2023).

6 Noel, R. L. *et al.* Getting ahead of Alzheimer's disease: early intervention with focused ultrasound. *Front Neurosci* **17**, 1229683 (2023).

7 Karakatsani, M. E. *et al.* Focused ultrasound mitigates pathology and improves spatial memory in Alzheimer's mice and patients. *Theranostics* **13**, 4102-4120 (2023).

8 Withington, C. G. & Turner, R. S. Amyloid-Related Imaging Abnormalities With Anti-amyloid Antibodies for the Treatment of Dementia Due to Alzheimer's Disease. *Front Neurol* **13**, 862369 (2022).

9 Hampel, H. *et al.* Amyloid-related imaging abnormalities (ARIA): radiological, biological and clinical characteristics. *Brain* **146**, 4414-4424 (2023).

10 Alector. *Alector Reports Fourth Quarter and Full Year 2021 Financial Results* (2022).

11 Alecou, T. *et al.* Amyloid beta Plaque Reduction With Antibodies Crossing the Blood-Brain Barrier, Which Was Opened in 3 Sessions of Focused Ultrasound in a Rabbit Model. *J Ultrasound Med* **36**, 2257-2270 (2017).

12 Downs, M. E. *et al.* Blood-Brain Barrier Opening in Behaving Non-Human Primates via Focused Ultrasound with Systemically Administered Microbubbles. *Sci Rep* **5**, 15076 (2015).

13 Yoon, K. *et al.* Localized Blood-Brain Barrier Opening in Ovine Model Using Image-Guided Transcranial Focused Ultrasound. *Ultrasound Med Biol* **45**, 2391-2404 (2019).

14 Blesa, J. *et al.* BBB opening with focused ultrasound in nonhuman primates and Parkinson's disease patients: Targeted AAV vector delivery and PET imaging. *Sci Adv* **9**, eadf4888 (2023).

15 Hughes, A. *et al.* Current and Emerging Systems for Focused Ultrasound-Mediated Blood-Brain Barrier Opening. *Ultrasound Med Biol* (2023).

16 Epelbaum, S. *et al.* Pilot study of repeated blood-brain barrier disruption in patients with mild Alzheimer's disease with an implantable ultrasound device. *Alzheimers Res Ther* **14**, 40 (2022).

17 Leinenga, G. & Gotz, J. Scanning ultrasound removes amyloid-beta and restores memory in an Alzheimer's disease mouse model. *Sci Transl Med* **7**, 278ra233 (2015).

18 Burgess, A. *et al.* Alzheimer disease in a mouse model: MR imaging-guided focused ultrasound targeted to the hippocampus opens the blood-brain barrier and improves pathologic abnormalities and behavior. *Radiology* **273**, 736-745 (2014).

19 Jordao, J. F. *et al.* Amyloid-beta plaque reduction, endogenous antibody delivery and glial activation by brain-targeted, transcranial focused ultrasound. *Exp Neurol* **248**, 16-29 (2013).

20 Lee, Y. *et al.* Improvement of glymphatic-lymphatic drainage of beta-amyloid by focused ultrasound in Alzheimer's disease model. *Sci Rep* **10**, 16144 (2020).

21 Poon, C. T. *et al.* Time course of focused ultrasound effects on beta-amyloid plaque pathology in the TgCRND8 mouse model of Alzheimer's disease. *Sci Rep* **8**, 14061 (2018).

22 Pandit, R. *et al.* Repeated ultrasound treatment of tau transgenic mice clears neuronal tau by autophagy and improves behavioral functions. *Theranostics* **9**, 3754-3767 (2019).

23 Kong, C. *et al.* Long-lasting restoration of memory function and hippocampal synaptic plasticity by focused ultrasound in Alzheimer's disease. *Brain Stimul* (2023).

24 Rigollet, S. *et al.* FUS-mediated BBB opening leads to transient perfusion decrease and inflammation without acute or chronic brain lesion. *Theranostics* **14**, 4147-4160 (2024).

25 (!!! INVALID CITATION !!! 13).

26 Ji, R. *et al.* Cavitation-modulated inflammatory response following focused ultrasound blood-brain barrier opening. *J Control Release* **337**, 458-471 (2021).

27 Kovacs, Z. I. *et al.* Disrupting the blood-brain barrier by focused ultrasound induces sterile inflammation. *Proc Natl Acad Sci U S A* **114**, E75-E84 (2017).

28 McMahon, D. & Hynynen, K. Acute Inflammatory Response Following Increased Blood-Brain Barrier Permeability Induced by Focused Ultrasound is Dependent on Microbubble Dose. *Theranostics* **7**, 3989-4000 (2017).
29 Kovacs, Z. I. *et al.* Focused ultrasound with microbubbles induces sterile inflammatory response proportional to the blood brain barrier opening: Attention to experimental conditions. *Theranostics* **8**, 2245-2248 (2018).
30 Martinez, P. J. *et al.* Comprehensive assessment of blood-brain barrier opening and sterile inflammatory response: unraveling the therapeutic window. *Sci Rep* **14**, 17036 (2024).
31 Lipsman, N. *et al.* Blood-brain barrier opening in Alzheimer's disease using MR-guided focused ultrasound. *Nat Commun* **9**, 2336 (2018).
32 Cohen, R. M. *et al.* A transgenic Alzheimer rat with plaques, tau pathology, behavioral impairment, oligomeric abeta, and frank neuronal loss. *J Neurosci* **33**, 6245-6256 (2013).
33 Gerstenmayer, M. *et al.* Acoustic Transmission Factor through the Rat Skull as a Function of Body Mass, Frequency and Position. *Ultrasound Med Biol* **44**, 2336-2344 (2018).
34 Magnin, R. *et al.* Magnetic resonance-guided motorized transcranial ultrasound system for blood-brain barrier permeabilization along arbitrary trajectories in rodents. *J Ther Ultrasound* **3**, 22 (2015).
35 Bankhead, P. *et al.* QuPath: Open source software for digital pathology image analysis. *Sci Rep* **7**, 16878 (2017).
36 Pascal, A. *et al.* Histologic evaluation of activation of acute inflammatory response in a mouse model following ultrasound-mediated blood-brain barrier using different acoustic pressures and microbubble doses. *Nanotheranostics* **4**, 210-223 (2020).
37 Kreisl, W. C. *et al.* (11)C-PBR28 binding to translocator protein increases with progression of Alzheimer's disease. *Neurobiol Aging* **44**, 53-61 (2016).
38 Tournier, B. B. *et al.* In Vivo TSPO Signal and Neuroinflammation in Alzheimer's Disease. *Cells* **9** (2020).
39 Tournier, B. B. *et al.* Astrocytic TSPO Upregulation Appears Before Microglial TSPO in Alzheimer's Disease. *J Alzheimers Dis* **77**, 1043-1056 (2020).
40 Tournier, B. B. *et al.* TSPO and amyloid deposits in sub-regions of the hippocampus in the 3xTgAD mouse model of Alzheimer's disease. *Neurobiol Dis* **121**, 95-105 (2019).
41 Smith, J. A. *et al.* Role of pro-inflammatory cytokines released from microglia in neurodegenerative diseases. *Brain Res Bull* **87**, 10-20 (2012).
42 Xu, L. *et al.* Microglia-Mediated Inflammation and Neurodegenerative Disease. *Mol Neurobiol* **53**, 6709-6715 (2016).
43 Gao, C. *et al.* Microglia in neurodegenerative diseases: mechanism and potential therapeutic targets. *Signal Transduct Target Ther* **8**, 359 (2023).
44 (!!! INVALID CITATION !!! 65).
45 Mildner, A. *et al.* P2Y(12) receptor is expressed on human microglia under physiological conditions throughout development and is sensitive to neuroinflammatory diseases. *Glia* **65**, 375-387 (2017).
46 Gomez Morillas, A. *et al.* Microglia and Neuroinflammation: What Place for P2RY12? *Int J Mol Sci* **22** (2021).
47 Lepiarz-Raba, I. *et al.* Metabolic regulation of microglial phagocytosis: Implications for Alzheimer's disease therapeutics. *Transl Neurodegener* **12**, 48 (2023).
48 Paolicelli, R. C. *et al.* Microglia states and nomenclature: A field at its crossroads. *Neuron* **110**, 3458-3483 (2022).
49 Csaszar, E. *et al.* Microglia modulate blood flow, neurovascular coupling, and hypoperfusion via purinergic actions. *J Exp Med* **219** (2022).
50 Walker, D. G. *et al.* Patterns of Expression of Purinergic Receptor P2RY12, a Putative Marker for Non-Activated Microglia, in Aged and Alzheimer's Disease Brains. *Int J Mol Sci* **21** (2020).
51 Bader, S. *et al.* Impact of Translocator Protein 18 kDa (TSPO) Deficiency on Mitochondrial Function and the Inflammatory State of Human C20 Microglia Cells. *Cells* **12** (2023).
52 Bae, K. R. *et al.* Translocator protein 18 kDa negatively regulates inflammation in microglia. *J Neuroimmune Pharmacol* **9**, 424-437 (2014).
53 Shoshan-Barmatz, V. *et al.* VDAC1 and the TSPO: Expression, Interactions, and Associated Functions in Health and Disease States. *Int J Mol Sci* **20** (2019).
54 Felmlee, M. A. *et al.* Monocarboxylate Transporters (SLC16): Function, Regulation, and Role in Health and Disease. *Pharmacol Rev* **72**, 466-485 (2020).
55 Halestrap, A. P. & Wilson, M. C. The monocarboxylate transporter family--role and regulation. *IUBMB Life* **64**, 109-119 (2012).

56 Wang, L. *et al.* Glucose transporter 1 critically controls microglial activation through facilitating glycolysis. *Mol Neurodegener* **14**, 2 (2019).
57 Lauro, C. & Limatola, C. Metabolic Reprograming of Microglia in the Regulation of the Innate Inflammatory Response. *Front Immunol* **11**, 493 (2020).
58 Bernier, L. P. *et al.* Microglial metabolic flexibility supports immune surveillance of the brain parenchyma. *Nat Commun* **11**, 1559 (2020).
59 Antoniou, A. *et al.* FUS-mediated blood-brain barrier disruption for delivering anti-Abeta antibodies in 5XFAD Alzheimer's disease mice. *J Ultrasound* (2023).
60 Scarcelli, T. *et al.* Stimulation of hippocampal neurogenesis by transcranial focused ultrasound and microbubbles in adult mice. *Brain Stimul* **7**, 304-307 (2014).
61 Kong, C. *et al.* Long-lasting restoration of memory function and hippocampal synaptic plasticity by focused ultrasound in Alzheimer's disease. *Brain Stimul* **16**, 857-866 (2023).
62 Ye, D. *et al.* Mechanically manipulating glymphatic transport by ultrasound combined with microbubbles. *Proc Natl Acad Sci U S A* **120**, e2212933120 (2023).
63 Majid, O. *et al.* Population pharmacokinetics and exposure-response analyses of safety (ARIA-E and isolated ARIA-H) of lecanemab in subjects with early Alzheimer's disease. *CPT Pharmacometrics Syst Pharmacol* (2024).
64 Jordao, J. F. *et al.* Antibodies targeted to the brain with image-guided focused ultrasound reduces amyloid-beta plaque load in the TgCRND8 mouse model of Alzheimer's disease. *PLoS One* **5**, e10549 (2010).
65 Nisbet, R. M. *et al.* Combined effects of scanning ultrasound and a tau-specific single chain antibody in a tau transgenic mouse model. *Brain* **140**, 1220-1230 (2017).
66 Janowicz, P. W. *et al.* Ultrasound-mediated blood-brain barrier opening enhances delivery of therapeutically relevant formats of a tau-specific antibody. *Sci Rep* **9**, 9255 (2019).
67 Dubey, S. *et al.* Clinically approved IVIg delivered to the hippocampus with focused ultrasound promotes neurogenesis in a model of Alzheimer's disease. *Proc Natl Acad Sci U S A* **117**, 32691-32700 (2020).
68 Antoniou, A. *et al.* FUS-mediated blood-brain barrier disruption for delivering anti-Abeta antibodies in 5XFAD Alzheimer's disease mice. *J Ultrasound* **27**, 251-262 (2024).
69 Bathini, P. *et al.* Acute Effects of Focused Ultrasound-Induced Blood-Brain Barrier Opening on Anti-Pyroglu3 Abeta Antibody Delivery and Immune Responses. *Biomolecules* **12** (2022).